Published for SISSA by Springer

Received: *December 16, 2015*
Revised: *January 22, 2016*
Accepted: *February 22, 2016*
Published: *March 3, 2016*

Hunting for neutral, long-lived exotica at the LHC using a missing transverse energy signature

Alexander Belyaev,[a] **Stefano Moretti,**[a] **Kilian Nickel,**[b] **Marc C. Thomas**[a] **and Ian Tomalin**[c]

[a] *School of Physics & Astronomy, University of S., Southampton SO17 1BJ, U.K.*

[b] *Bethe Center for Theoretical Physics & Physikalisches Institut der Universität Bonn, 53115 Bonn, Germany*

[c] *Rutherford Appleton Laboratory, Science & Technology Facilities Council (STFC), Chilton, Didcot. Oxon OX11 0QX, U.K.*

E-mail: a.belyaev@soton.ac.uk, s.moretti@soton.ac.uk, nickel@th.physik.uni-bonn.de, m.c.thomas@soton.ac.uk, ian.tomalin@stfc.ac.uk

Abstract: Searches at the Large Hadron Collider (LHC) for neutral, long-lived particles have historically relied on the detection of displaced particles produced by their decay *within* the detector volume. In this paper we study the potential of the complementary signature comprising of the missing transverse energy ($E_T^{\rm miss}$) signal, traditionally used to look for dark matter, e.g., the lightest supersymmetric particle (LSP), to extend the LHC coverage to models with long-lived (LL) particles when they decay *outside* the detector. Using CMS and ATLAS analyses at the 8 TeV LHC, we set an upper limit at the 95% confidence level (CL) on the production cross sections for two specific scenarios: (i) a model with a heavy non-standard model Higgs boson decaying to a LL scalar and (ii) an R-parity violating (RPV) SUSY model with a LL neutralino. We show that this method can significantly extend the LHC sensitivity to neutral, LL particles with arbitrary large lifetimes and that the limits obtained from a $E_T^{\rm miss}$ signal are comparable to those from displaced particle searches for decay distances above a few meters. Results obtained in this study do not depend on the specific decay channel of the LL particle and therefore are model-independent in this sense. We provide limits for the whole two-dimensional plane in terms of the mass of the LL particle and the mass of the mediator up to masses of 2 TeV including particular benchmarks studied in the original experimental papers. We have made these limits available in the form of a grid which can be used for the interpretation of various other new physics models.

Keywords: Phenomenological Models, Supersymmetry Phenomenology

ArXiv ePrint: 1512.02229

doi:10.1007/JHEP03(2016)018

JHEP03(2016)018

Contents

JHEP03(2016)018

1 Introduction

New long-lived (LL) particles are predicted by various Beyond Standard Model (BSM) scenarios, such as neutralinos in Supersymmetry (SUSY) with weak R-parity violation [1], gluinos in split-SUSY [2], "hidden valley" models [3], heavy photons in Little Higgs models with T-parity [4, 5] broken by a Wess-Zumino-Witten anomaly term [6] and LL heavy neutrinos in the minimal $B - L$ extension of the Standard Model (SM) [7].

In this paper, we focus on the case of neutral LL particles. Searches for neutral LL particles at the LHC have historically been reliant on reconstructing their decay products within the detector volume. If the LL particle lifetime is of order picoseconds to nanoseconds, then its decay can yield striking signatures of displaced leptons, jets, photons or charged tracks. Numerous searches for these signatures have been performed at the LHC, exemplified by [8–10] (CMS) and [11, 12] (ATLAS). However, for longer lifetimes, an increasing proportion of the LL particles decay outside the detector, reducing the efficiency of these searches and leading to correspondingly weaker cross section limits.

In this paper, we extend existing limits to arbitrarily long lifetimes, by exploiting the fact that neutral, LL particles that decay outside the detector will be visible as missing transverse energy, E_T^{miss}. As such, our approach is complementary to the traditional one exploiting displaced particles. In fact, the cross section limits obtained using the E_T^{miss} signature will improve with increasing lifetime, as a larger proportion of particles decay outside the detector.

To illustrate this method, we concentrate on the results of two CMS papers, which searched for displaced vertices reconstructed within the CMS tracker, produced by either

two leptons [9] or a quark-antiquark pair [10]. In both these papers, limits were set for a number of benchmark points for two specific models: (i) a simplified model with a heavy, non-SM Higgs boson H^0 decaying into two LL scalar bosons X which then decay exclusively to either e^+e^-, $\mu^+\mu^-$ or $q\bar{q}$ and (ii) a SUSY model with a LL neutralino $\tilde{\chi}^0$ decaying via a R-parity violating coupling exclusively to either $\ell^+\ell^-\nu$ or $q\bar{q}^{(\prime)}\mu$ (with the prime indicating different quark flavours). For both of these models, we use measurements of the E_T^{miss} signature from CMS and ATLAS analyses at 8 TeV, to set upper bounds on signal cross sections for each decay channel, assuming that the LL particle is stable. Using the geometric properties of the detectors and the energy and rapidity distribution of the LL particle, we then extrapolate these cross section limits to finite lifetimes including when the mean decay distance is within the detector. For each benchmark point in these CMS papers, we have extended the limits such that an upper limit on the cross section is provided for any lifetime from around 10^{-2} cm (depending on benchmark point) up to arbitrarily long lifetimes. We show that for these models, analysis of E_T^{miss} signature can set more stringent cross section limits than displaced vertex searches for a LL particle with a lifetime of order a few nanoseconds and longer. Upper limits over a range of masses of the LL particle and its mediator are also provided for both models, under the assumption that the LL particle has a lifetime such that it always decays outside the detector.

The rest of the paper is organised as follows. In section 2 we discuss the models, signal simulation and details of the analyses. The results are given in section 3, followed by our conclusions in section 4.

2 Setup

2.1 Models

To best demonstrate how E_T^{miss} signatures can be used to extend to longer particle lifetimes, the cross section limits obtained from LHC displaced particle searches, we use the same signal models that were studied by CMS in [9, 10]. Both these CMS papers considered the same pair of signal models, examining LL particle decays to leptonic [9] or hadronic [10] final states, respectively.

It is important to stress whereas in the CMS simulations, the LL particles were allowed to decay, for our E_T^{miss} study, we instead use simulations in which they are defined as completely stable. This is because we (conservatively) assume that neutral LL particles only contribute to the E_T^{miss} signature if they both leave the detector before decaying. As a result, which final state they eventually decay to is completely irrelevant to the E_T^{miss} study. This makes our analysis much more model-independent than traditional displaced particle searches at the LHC. Further, our analysis does not depend on the reconstruction or identification efficiencies of the LL particle decay products, which allows us to have good sensitivity to the signature under study.

The two signal models are as follows.

(1) A simplified model with a heavy, non-SM Higgs boson H^0 produced via gluon fusion (via an effective vertex from $\frac{1}{2}\text{Tr}[G^2]H$, with H being a new singlet) and decaying

JHEP03(2016)018

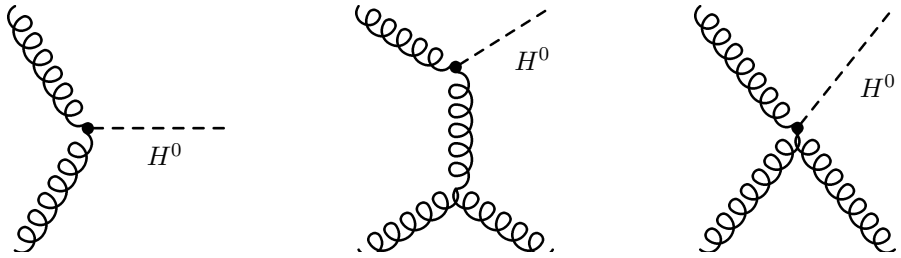

Figure 1. Production of H^0 in the HXX model, including up to 1 jet in the final state.

to two long-lived, heavy, neutral, spinless bosons X. In the CMS analyses, these subsequently decay either to two leptons [9] or a quark-antiquark pair [10], whereas our simulation treats them as stable, as explained above.

$$gg \to H \to XX \tag{2.1}$$

$$X \to e^+e^-, \mu^+\mu^-, q\bar{q} \quad \text{(in the CMS analyses)} \tag{2.2}$$

The respective production diagrams are shown in figure 1. The decay width of the heavy Higgs is assumed to be much smaller than its mass, $\Gamma_H \ll m_H$ and so we use the narrow width approximation. Thus we only consider processes where the heavy Higgs is produced on-shell and the mass relation $m_X \leq \frac{1}{2}m_H$ holds. We will refer to this model as HXX for short.

(2) A SUSY model with small R-parity violating (RPV) couplings which give rise to a LL neutralino $\tilde{\chi}^0$. A pair of squarks $\tilde{q}$ of arbitrary flavour ($\tilde{u}_L$) is strongly produced and decays into a quark q and a neutralino $\tilde{\chi}^0$,

$$pp \to \tilde{q}\tilde{q}^*, \qquad \tilde{q} \to q\tilde{\chi}^0. \tag{2.3}$$

In the CMS analyses, the neutralino decays either to $\ell^+\ell^-\nu$ [9] or to $u\bar{d}\mu^-$ [10], via $\lambda_{ijk}\hat{L}_i\hat{L}_j\hat{E}_k$ or $\lambda'_{ijk}\hat{L}_i\hat{Q}_j\hat{D}^c_k$ R-parity violating terms, respectively [1]. Our simulation instead treats the neutralino as stable, as explained above. The diagrams for the strong production of the squark pair are shown in figure 2. There are three types of squark pairs: $\tilde{q}\tilde{q}$, $\tilde{q}\tilde{q}^*$ or $\tilde{q}^*\tilde{q}^*$. We denote these squark pairs as $\tilde{Q}\tilde{Q}$ with $\tilde{Q} = \tilde{q}, \tilde{q}^*$. The branching ratio of $\tilde{q} \to q\tilde{\chi}^0$ is assumed 1 for all events.

2.2 Event generation

As we have already mentioned, we look for signals where the neutral LL particle (X or $\tilde{\chi}^0$) leaves the detector before decaying. For the HXX model the only way to observe the E_T^{miss} signal is to use events with a high P_T jet from initial state radiation (ISR) induced by strong interactions. In this case this high P_T jet will be recoiling against the pair of XX neutral LL particles providing a classic mono-jet signature for XX decaying outside of detector. In case of the RPV SUSY scenario, if the squark and neutralino have a small mass gap, one can again rely on a mono-jet signature. In contrast, if the mass gap is

JHEP03(2016)018

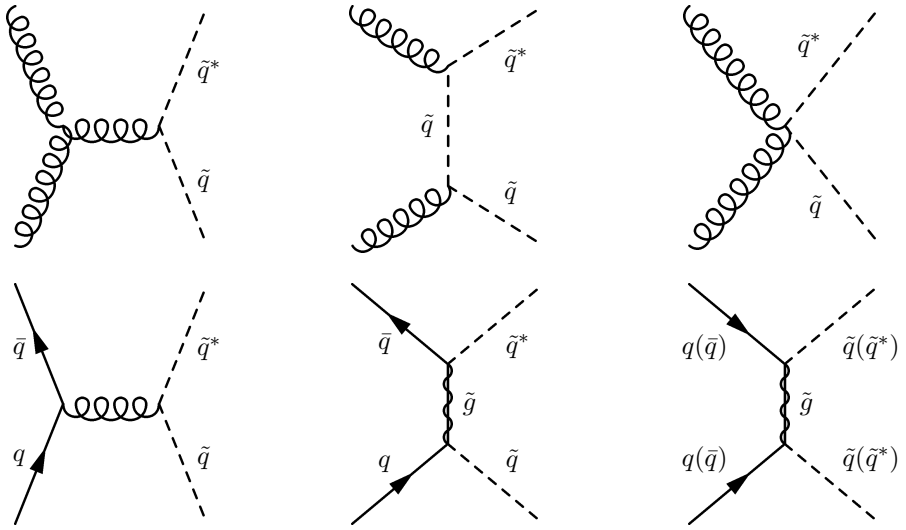

Figure 2. Strong production of squark pairs in SUSY.

large, then the squark will decay to a SM quark and a neutralino, which would lead to a 'E_T^{miss} + jets' signature. The signal events for both of the models in 2.1 were generated by `MadGraph5 v2.1.2` [13] with `Pythia 6.4` [14, 15] for parton showering and hadronisation.

For the RPV-SUSY model, we use the default `mssm` model from `MadGraph` (because we only consider signatures where the neutralino decays outside the detector) and used $\tilde{q} = \tilde{u}_L$ without loss of generality to generate the strong production of squark pairs $\widetilde{qq}$, $\widetilde{q}^*\widetilde{q}^*$ and $\widetilde{q}\widetilde{q}^*$ (which we denote as $\tilde{Q}\tilde{Q}$) decaying via $\widetilde{q} \to q\tilde{\chi}_1^0$ ($\widetilde{q}^* \to \bar{q}\tilde{\chi}_1^0$). In order to ensure accurate simulation of hard ISR jets, we allow an additional matrix element jet in our event generation which is matched using the k_T MLM scheme [15]. All SUSY masses (except $m_{\tilde{\chi}^0}, m_{\tilde{q}}$) including the gluino mass are set to 5 TeV to match the model used by CMS.

The HXX scenario described in section 2.1 was implemented using a model generated using the LanHEP package [16–18], with an effective vertex between gluons and the heavy Higgs implemented via a $\frac{1}{2}\text{Tr}[G^2]H$ Lagrangian term, where G is the usual gluon field strength tensor. Again k_T MLM matching between 0-jet and 1-jet events was used to ensure accurate simulation of the hard jets.

2.3 Used CMS and ATLAS E_T^{miss} analyses

Signatures with E_T^{miss} have been the focus of the dedicated papers by ATLAS and CMS, mainly is the context of SUSY searches involving the LSP. These papers present results for various final states produced in association with the E_T^{miss}. Which paper allows us to place the strongest cross section limits on the two signal models we consider will depend both on the model and on the particle masses. We therefore need to implement and use multiple such publications to ensure that we place the tightest bounds possible over the range of masses in our models. Fortunately, the results of a large number of such papers have already been implemented in the `CheckMATE` [19–27] framework, which allows easy use of the implemented searches. This tool takes a given sample of Monte Carlo events

JHEP03(2016)018

in the HEP or HEPMC format after PYTHIA/HERWIG level of simulation and performs a detector simulation for the sample using `Delphes-3` [20]. `CheckMATE` is then able to apply in turn each analysis as described in the experimental papers to the generated signal event. The resulting efficiencies along with information provided by the publication, such as the 95% C.L. on signal count $S^{95}_{\rm exp}$, is used to produce results from which we can find the cross-section limit placed on our model by each analysis. Those analyses which we used have all been validated by using published results including available cut-flows.

For each paper, CMS and ATLAS typically give results for a number of different signal regions, for example, defined by different $E_T^{\rm miss}$ requirements. We will refer to these as 'analysis sets'. When we place limits on one of our signal models for given particle masses, we only use the results of the best analysis set within the best paper, where 'best' is defined as the one yielding the strongest *expected limit*. By using the expected limit instead of the observed one, we avoid the 'look elsewhere' effect. In producing our limits, we do not account for any systematic uncertainty on the new physics signal selection efficiency, as this would be model dependent.

From the long list of available papers, three are particularly important, setting the best limits for the models we studied. A very brief outline of the selection cuts and analysis sets of these three is given below. (A fourth paper, a monojet analysis by CMS [28], is potentially interesting, but not yet available inside `CheckMATE`).

1. ATLAS $E_T^{\rm miss}$ + multi-jet analysis [29].
   It uses $20.3\,{\rm fb}^{-1}$ of $\sqrt{s} = 8\,{\rm TeV}$ data. $E_T^{\rm miss}$ must be above 160 GeV, the leading jet must have $p_T(j_1) > 130\,{\rm GeV}$ and the second leading jet $p_T(j_2) > 60\,{\rm GeV}$. The analysis sets are distinguished by jet multiplicity 2,3,4,5,6, corresponding to analysis set codes *A,B,C,D,E*, while only jets with $p_T > 60\,{\rm GeV}$ are valid in this count. Given one of these five categories, signals are then subjected to *loose (L), medium (M)* or *tight (T)* constraints. In our case, analysis sets *AM, BM, BT, CM, CT* are relevant. For full details, cf. page 3, table 1 of [29].

2. ATLAS $E_T^{\rm miss}$ + monojet analysis [30].
   It uses $20.3\,{\rm fb}^{-1}$ of $\sqrt{s} = 8\,{\rm TeV}$ data. Events must have at least one jet with $p_T > 120\,{\rm GeV}$ and $|\eta| < 2.0$ and no charged leptons (of $p_T > 7\,{\rm GeV}$). For the leading jet, $p_T/E_T^{\rm miss} > 0.5$ must hold ($E_T^{\rm miss} > 150\,{\rm GeV}$ required). The number of jets is unrestricted, but the leading jet is only considered (monojet-like selection). Nine analysis sets are defined between $150\,{\rm GeV} < E_T^{\rm miss} < 700\,{\rm GeV}$, labelled *SR1* through *SR9*. Complete definitions, cf. page 7, table 2, of [30].

3. CMS analysis using the α_T variable [31].
   It uses $11.7\,{\rm fb}^{-1}$ of $\sqrt{s} = 8\,{\rm TeV}$ data. Instead of $E_T^{\rm miss}$, this analysis uses the related variable α_T [32, 33] to suppress multijet background events. This variable is used to be more independent of mismeasurements of $E_T^{\rm miss}$. For two back-to-back jets with $E_T^{j_1} = E_T^{j_2}$, α_T is equal to 0.5. A value greater than 0.5 signifies that the jets are recoiling against significant $E_T^{\rm miss}$. For further details of the α_T variable see [31–33]. Events with e or μ with $p_T > 10\,{\rm GeV}$ are vetoed as well as those with an isolated

JHEP03(2016)018

photon with $p_T < 25\,\text{GeV}$. To cut out multijet background events, $\alpha_T > 0.55$ is required. Also, the scalar sum of all transverse jet energies, $H_T = \sum_{i=1}^{n_{\text{jet}}} E_T^{j_i}$, must be larger than 275 GeV. The two leading jets must each have $p_T > 100\,\text{GeV}$ and the leading jet satisfies $|\eta| < 2.5$, but these conditions are also relaxed for some analysis sets. The analysis sets are named after the number of jets (`23j_` for 2-3 jets or `4j_` for ≥ 4 jets) + number of b-jets (`0b_` or `1b_`) + lower limit of H_T bin (`275, 325, 375, 475` etc.). Example: `23j_0b_325`.

2.4 Escape probability

In order to find the production cross section limits for long-lived particle pairs with a given lifetime, we calculate the proportion of events passing analysis cuts where both particles decay outside the detector, producing a missing transverse energy signature, and use this along with the limits if the same particles were stable, calculated as discussed in section 2.3, to find the 95% cross section limits as a function of the lifetime.

In order to achieve this, we edited the `CheckMATE` code, so that for each simulated event which passed all of the selection cuts, we calculate for each LL particle the probability of it leaving the detector before decaying. This probability is

$$p(D) = \exp\left(\frac{-D}{c\beta\gamma\tau}\right) \tag{2.4}$$

where D is the distance the particle must travel to leave the detector undecayed (distance from the interaction point to the periphery of the detector), being a function of the size and shape of the detector and the rapidity of the LL particle, while β, γ, and τ are the usual relativistic factors and the lifetime of the particle. The dependence of D versus the pseudorapidity η is shown in figure 3. For this calculation, the ATLAS and CMS detectors are assumed to be cylindrical in shape, with ATLAS having a length of 46 m and a diameter of 25 m, and CMS having a length of 21 m and a diameter of 15 m. The event is subsequently weighted according to probability that both LL particles leaving the detector undecayed,

$$w = p_1(D_1)p_2(D_2). \tag{2.5}$$

with p_1, p_2 denoting the probabilities for particle 1 and 2 respectively. Summing these weights allows us to calculate the proportion, P, of these events which would have given an E_T^{miss} signature. We are thus able to calculate the 95% C.L. on the signal cross section for any arbitrary lifetime,

$$\sigma_{c\tau}^{95\%} = \frac{1}{P}\sigma_{\text{stable}}^{95\%} \tag{2.6}$$

where $\sigma_{\text{stable}}^{95\%}$ is the cross section limits calculated using `CheckMATE` by assuming that all the LL particles decay outside the detector as described in section 2.3. There is a simpler approximation to obtain the lifetime dependent limit $\sigma_{c\tau}^{95\%}$, which is suitable for other researchers who wish to quickly approximate similar limits as those presented in figures 4–5. This method requires only an energy distribution of the LL particles and is described in detail in the appendix A. We found this method to give a reasonably agreement with our more accurate results. It can be applied to the limits provided by our grid results. N.B.

JHEP03(2016)018

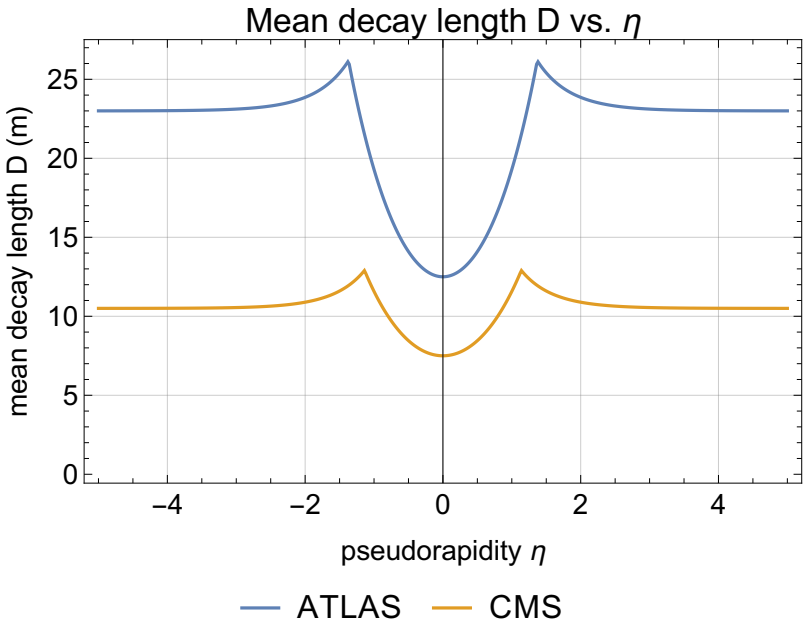

Figure 3. Dependence of the mean decay length D on η for ATLAS and CMS. The value of $D(\eta = 0)$ corresponds to the detector's radius and $D(|\eta| > 5)$ to the half length.

Events where only one LL particle exits the detector before decaying are also likely to yield a missing transverse energy signature, and could therefore be used to improve the limits obtained with this signature, particularly for smaller particle lifetimes. However, this has not been done here, because to do so would require an understanding of how the ATLAS and CMS detectors would react to the other LL particle: the one decaying within the detector volume. Whether the decay products of this particle contribute to the visible energy in the event depends on details of their event reconstruction algorithms and on the selection requirements of their missing transverse energy publications.

3 Results

We have performed analyses using the E_T^{miss} signature for the benchmark points (BPs) used in the CMS studies [9] and [10] of the displaced vertices, where the BPs correspond to various particle masses in the two signal models. As a result we have obtained the cross section limits $\sigma_{\text{stable}}^{95\%}$, i.e., the cross section for $c\tau \to \infty$ for both models for the $\sigma(pp \to H^0 \to XX)$ and $\sigma(pp \to \widetilde{Q}\widetilde{Q} \to \tilde{\chi}^0\tilde{\chi}^0 + \text{jets})$ processes, respectively. The results for the HXX model are shown in table 1 and for the RPV-SUSY model in table 2, where we indicate the analysis set which provides the best sensitivity for each point. For the HXX model, for every BP, the ATLAS monojet + E_T^{miss} paper [30] provides the best sensitivity. This can be understood from the fact that the heavy Higgs is produced on-shell from gluon fusion and then decays to two back-to-back X bosons (in the heavy Higgs rest frame), resulting in very little E_T^{miss} unless the heavy Higgs is boosted as a result recoiling against

JHEP03(2016)018

Benchmark Point	m_H (GeV)	m_X (GeV)	$\sigma^{95\%}_{\text{stable}}$ (pb)	Analysis — SR
1a	125	20	38.3	ATLAS monojet [30] - SR4
1b	125	50	39.9	ATLAS monojet [30] - SR4
2a	200	20	17.1	ATLAS monojet [30] - SR4
2b	200	50	17.5	ATLAS monojet [30] - SR4
3a	400	20	3.29	ATLAS monojet [30] - SR6
3b	400	50	3.17	ATLAS monojet [30] - SR6
3c	400	150	3.16	ATLAS monojet [30] - SR6
4a	1000	20	0.94	ATLAS monojet [30] - SR7
4b	1000	50	0.96	ATLAS monojet [30] - SR7
4c	1000	150	0.94	ATLAS monojet [30] - SR7
4d	1000	350	0.97	ATLAS monojet [30] - SR7

Table 1. Benchmark points from [9] and [10] (Model 1, HXX) and their 95% CL upper limit on cross section, together with the CMS or ATLAS E_T^{miss} paper from which this limit was derived.

Benchmark Point	$m_{\tilde{q}}$ (GeV)	$m_{\tilde{\chi}^0}$ (GeV)	$\sigma^{95\%}_{\text{stable}}$ (pb)	Analysis — SR
1	120	48	33.5	CMS α_T [31] - 4j_0b_325
2	350	148	0.57	CMS α_T [31] - 23j_0b_325
3	700	150	0.041	ATLAS multijet [29] - AM
4	700	500	0.24	CMS α_T [31] - 23j_0b_375
5	1000	148	0.0086	ATLAS multijet [29] - AM
6	1000	500	0.025	ATLAS multijet [29] - AM
7	1500	150	0.0018	ATLAS multijet [29] - CT
8	1500	494	0.0024	ATLAS multijet [29] - CT

Table 2. Benchmark points from [9] and [10] (Model 2, RPV-SUSY model) and their 95% CL upper limit on cross section, together with the CMS or ATLAS E_T^{miss} paper from which this limit was derived.

a jet from initial state radiation (ISR). For the RPV-SUSY model, the paper providing the best limit depends on the BP. For $m_{\tilde{q}} = 120, 350$, the CMS paper [31], which uses the α_T variable, provides the best limit. On the other hand, for $m_{\tilde{q}} = 1000, 1500\,\text{GeV}$, the best limit is provided by using the ATLAS paper [29], which studies a large E_T^{miss} + multi-jet signal. Since in this model, squarks are produced which then each decay to a quark and a LL particle, the presence of E_T^{miss} is not dependent on ISR in this case, so papers allowing for multiple jets in association with E_T^{miss} provide the best limits. The obtained for the HXX model are significantly weaker than those obtained for the RPV-SUSY model, because only a small fraction of events contain the hard ISR on which the HXX limits rely.

JHEP03(2016)018

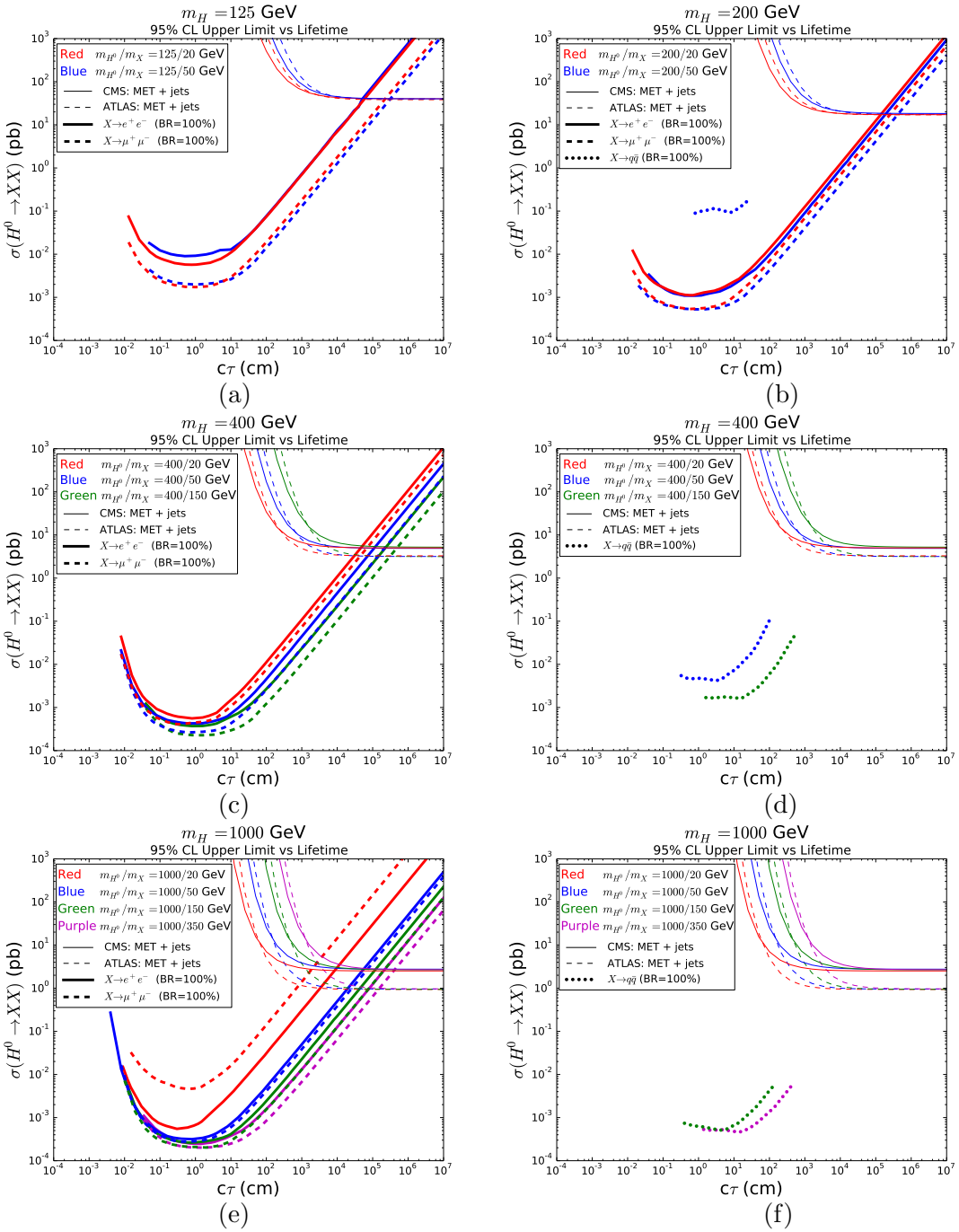

Figure 4. 95% CL upper limits on cross sections for the heavy Higgs model (HXX) with m_H = 125 GeV (a), 200 GeV (b), 400 GeV (c,d) and 1000 GeV (e,f). The colour red (blue) indicates $m_X = 20\,\text{GeV}$ (50 GeV) *for all curves*. The thin curves in the upper-right corner of all figures show our new E_T^{miss}-derived limits on LL particle cross sections for each detector (solid: CMS, dashed: ATLAS). For comparison, the cross section limits from the CMS displaced vertex searches, under the assumption of 100% branching ratios, are shown by thick curves: displaced leptons searches ($X \to \ell^+\ell^-$) [9] are indicated by the solid curves for $\ell = e$ and by dashed curves for $\ell = \mu$; whereas displaced jet searches ($X \to q\bar{q}$) [10] are indicated by dotted curves. Our new limits are identical in (c) and (d) as well as in (e) and (f) and have been split for clarity.

JHEP03(2016)018

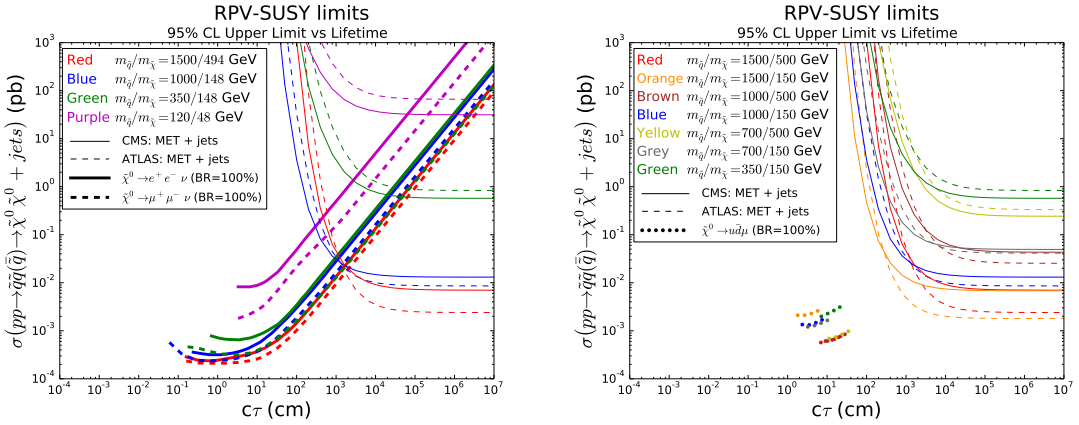

(a) (b)

Figure 5. 95% CL upper limits on cross sections for the RPV-SUSY model with colours indicating various mass points. The thin curves in the upper-right corner of both (a) and (b) show our new E_T^{miss}-derived limits on LL particle cross sections for each detector (solid: CMS, dashed: ATLAS). For comparison, the cross section limits from the CMS displaced vertex searches, under the assumption of 100% branching ratios are shown by thick curves: (a) for displaced dilepton searches ($\tilde{\chi}^0 \to \ell^+\ell^-\nu$) [9], with the solid curves indicating $\ell = e$ and the dashed curves indicating $\ell = \mu$; and (b) for displaced dijet searches [10] searches ($\tilde{\chi}^0 \to u\bar{d}\mu$) shown by dotted curves.

We subsequently calculate the upper 95% CL on cross sections, $\sigma_{c\tau}^{95\%}$, for arbitrary lifetimes by performing the procedure described in section 2.4. These results are plotted in figures 4, 5, where figure 4 show results for the HXX model for BPs with a heavy Higgs mass, m_H of 125 GeV, 200 GeV, 400 GeV and 1000 GeV, and figure 5 displays the results for the RPV-SUSY model. Each colour corresponds to a different BP, with the thin solid curves denoting the limits found using the dimensions of the CMS detector and using the CMS analyses, and the dashed thin line corresponding to the equivalent ATLAS limits. For comparison, we also plot the published results from the CMS displaced vertex analyses [9, 10] in thick curves (either solid, dashed or dotted). Beyond a certain lifetime, the cross section limits for the displaced vertex signatures increase in proportion to a power of the LL particle lifetime, and so appear on the log-log plot as a straight line. This can be understood from the following consideration. Using a simplified picture and assuming that the detector only has non-zero acceptance for particles decaying within a distance L from the centre of the detector, the probability that a LL particle of momentum P and mass M decays within this acceptance region is $1 - \exp(\frac{-LM}{Pc\tau})$, which tends to $\frac{-LM}{Pc\tau}$ in the long lifetime limit. Cross section limits will scale in inverse proportion to the acceptance. An analysis such as the CMS displaced dilepton vertex search [9], which relies on the reconstruction of the decay products of just one LL particle per event will thus yield cross section limits that scale in proportion to τ in the large τ limit. This consideration allowed us to extrapolate these CMS limits to longer lifetimes than in their original publication, providing that the original results reached long enough lifetimes for this scaling behaviour to be observed. We did not attempt this for the CMS displaced dijet vertex search [10], because the original publication did not reach sufficiently long enough lifetimes in that case.

JHEP03(2016)018

The results show that, although the minimum cross section limits (occurring at $c\tau = \mathcal{O}(1\text{ cm})$) from displaced vertex searches are of order a fb, and those from the E_T^{miss} searches are of order a pb or more, the sensitivity to LL particles from the E_T^{miss} signature can be better than from displaced vertex searches for comparatively large times starting from $c\tau$ about 10^3 cm (for the RPV-SUSY model with decays to $e^+e^-\nu$ - see figure 5, BP $m_{\tilde{q}}/m_{\tilde{\chi}^0} = 120/48\,\text{GeV}$). However, generally the limits become comparable for $c\tau$ of $\mathcal{O}(10^4 - 10^5\text{ cm})$.

When making such comparisons, it is important to note that in figures 4 and 5, the limits presented for the CMS displaced vertex searches are assuming a branching ratio of 1 of the LL particle to its respective decay, whilst our limit using E_T^{miss} searches is independent of decay channels or branching ratios. As an example, this means that in a realistic scenario where the LL X-particle has a branching ratio of 0.01 to e^+e^-, the presented CMS displaced vertex limits would be weakened by 2 orders of magnitude, and the limits from E_T^{miss} signals would therefore be comparable for proper decay lengths as low a 1 metre or less for certain benchmark points. This highlights the fact that the limits set using E_T^{miss} are less model dependent than those for displaced vertices, thus they represent a new and complementary tool of investigation.

One should note about the results in figures 4 and 5 that, even when ATLAS provide the best result for $\sigma_{\text{stable}}^{95\%}$, due to the smaller size of CMS, a larger proportion of the decays will occur outside the detector for a specific BP as compared to the ATLAS detector, and therefore for small enough $c\tau$, CMS limits become better than those of ATLAS. This demonstrates an important complementarity of two detectors. Furthermore, the effect of the LL particle mass is visible, because this effects the relativistic γ-factor and therefore its lifetime in the lab-frame. As an example, in figure 4(e,f), cross section limits for each BP for large $c\tau$ are of the same order of magnitude where near 100% of decays occur outside the detector for each m_X. However for smaller $c\tau$ there is a clear pattern of limits for BPs with lower m_X extending further left into the low $c\tau$ region because of the relativistic time-dilation.

To provide a more comprehensive result than only the BPs for these two models, we also present our results for $\sigma_{\text{stable}}^{95\%}$ in the form of a m_{mediator} vs m_{LL} plane. These are shown in figure 6 for the HXX model and figure 7 for the RPV-SUSY model, where the $\sigma_{\text{stable}}^{95\%}$ upper limits are indicated by the colour chart. In order to avoid large statistical errors, for some points, most notably those with small $m_{\tilde{q}}$, we were required to generate very large numbers of Monte Carlo events. It is interesting to note the different pattern of results observed between the HXX model in figure 6, where the cross section limits depend exclusively on the mass of the heavy Higgs (m_H) mediating the LL X production (with small statistical fluctuations) and the RPV-SUSY model in figure 7, where the limits depend largely on the mass gap $\Delta m = m_{\tilde{q}} - m_{\tilde{\chi}^0}$.

These differences can be explained by the production and decay channels of the two models. In the HXX model, the heavy Higgs, H is produced on-shell, before decaying into two X bosons, and therefore, the E_T^{miss} is just the p_T of the H. As m_H increases, so does its average p_T, and therefore so does the E_T^{miss} on which the analysis depends, leading to more stringent cross section bounds with larger m_H.

In the RPV-SUSY model on the other hand, each squark decays into a neutralino and quark ($\tilde{q} \to q\tilde{\chi}^0$), giving a signal of E_T^{miss} and jets. For small mass gaps between the squark

JHEP03(2016)018

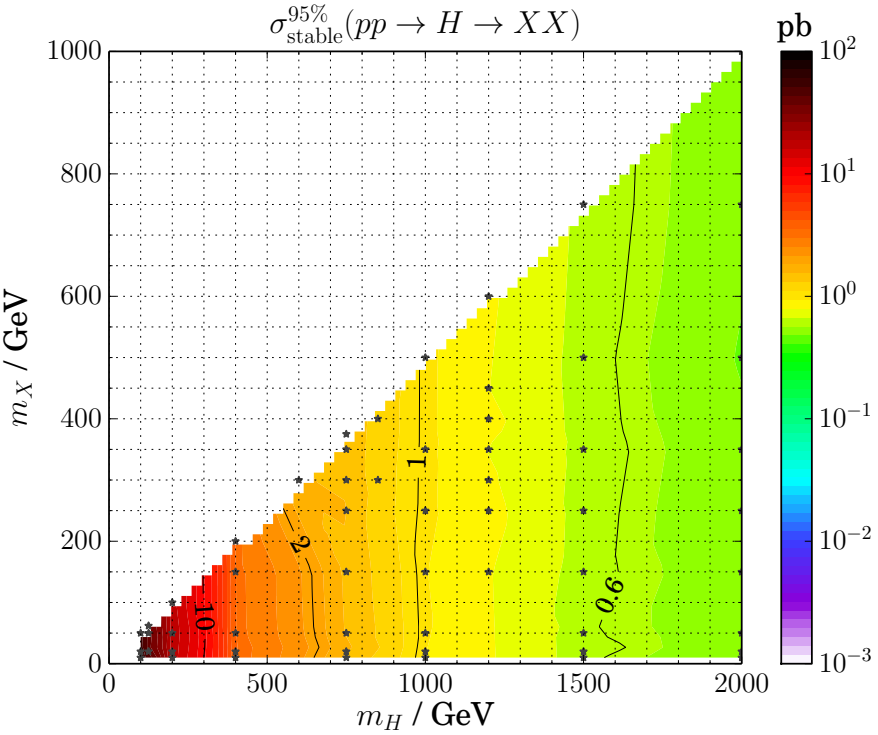

Figure 6. The figure shows the upper limit of the production cross section of XX+jets final states for the HXX-model in units of pb. The x-axis shows the mass of the mediator H and the y-axis shows the mass of the LL X particle.

and the neutralino, Δm, the decay products tend to be soft, giving a low E_T^{miss}, soft jets and a low signal efficiency. In this case, the best limits come from the monojet analysis (or α_T analyses with 2-jet signatures for low values of $m_{\tilde{q}}$) and are of similar size as for the Higgs boson model (figure 10 in the appendix shows the best analysis sets of the ATLAS monojet analysis for each sample point). As Δm increases, the E_T^{miss} and jet p_T increase too, increasing the signal cut efficiency and improving the cross section limits. Therefore the most important parameter for the RPV-SUSY model is $\Delta m = m_{\tilde{q}} - m_{\tilde{\chi}}$ as is clearly seen in figure 7.

At this point it is worth noting that, whilst we have been working with the HXX model (described in section 2.1) which specifically has a scalar LL particle X, these limits are valid regardless of the spin or decay pattern of X and are in fact valid for any model where the production of a scalar, H, with a narrow width decaying to a LL particle can be described by the effective vertex $\frac{1}{2}\text{Tr}[G^2]H$. This is because the H is a scalar which is produced on-shell, then decays to X pairs isotropically in its rest frame, which then leaves the detector before decaying (for our E_T^{miss} signal), meaning that the spin of X is not relevant.

We should also stress that as we did not simulate displaced vertices explicitly, we do not consider events where one of the particles decay within, and the other outside detector and as a result our limits are conservative. This could potentially give an additional E_T^{miss} signature, particularly for the HXX model where the signal would no longer be suppressed

JHEP03(2016)018

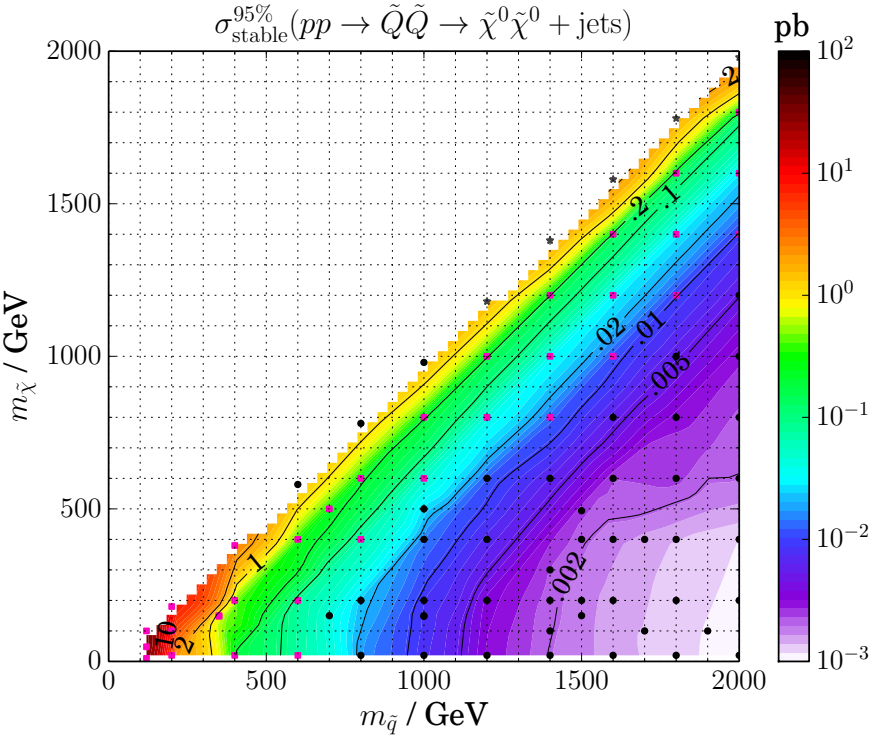

Figure 7. The figure shows the upper limit of the production cross section of $\tilde{\chi}^0\tilde{\chi}^0$+jets final states for the MSSM in units of pb. The x-axis shows the mass of the $\tilde{q}$ squark and the y-axis shows the mass of the neutralino $\tilde{\chi}^0$ (LSP). Black dots indicate sample points where the ATLAS multijet paper [29] performed best, grey stars indicate the ATLAS monojet paper [30], and pink squares indicate best performance with the CMS α_T paper [31]. A similar plot showing the different signal regions is shown in the appendix, figure 10.

by the requirement of recoiling against a high-p_T jet. Simulations, in particular detector simulations, involving displaced vertices are more technically difficult and therefore was beyond the scope of this study. However as this scenario has the potential to produce strong limits, the authors would like to encourage experimentalists to consider such scenarios.

4 Conclusion

CMS and ATLAS have historically searched for long-lived, neutral particles by looking for evidence of their decay products within the detector. We have demonstrated that using missing transverse energy (E_T^{miss}) analyses, which are traditionally used for dark matter searches, it is possible to complement these existing LHC searches, extending the cross section limits on long-lived, neutral particles to arbitrarily long lifetimes. We have illustrated this by using E_T^{miss} signatures to place cross section limits on two signal models considered in CMS searches for displaced leptons or jets produced by long-lived particle decay [9, 10]. The limits we obtained using E_T^{miss} are comparable to those from the displaced lepton/jet searches for $c\tau$ values as short as order of a few metres (lifetime of order of a

JHEP03(2016)018

nanosecond), although for the majority of benchmark points, they become comparable at larger distances of $\mathcal{O}$(10m - 100m) which is the order of the detector size and larger. However it is important to note that whilst our limits on the production cross sections of the LL particles are independent of how the particle decays, the CMS displaced vertex limits depend on the branching ratios to the channels considered. For realistic branching ratios of order a few percent or less, the CMS limits from displaced vertex searches would be considerably weakened and limits from E_T^{miss} become much more competitive. In this case our cross section limits for stable particles can be better then the minimum obtained (for any $c\tau$) from displaced vertex searches, and our new limits can be comparable to those from the displaced vertex searches for decay distances less than 1 metre.

In the case of a model where a heavy Higgs boson decays to a long-lived, neutral scalar, we used predominantly an ATLAS study of events with a monojet and large E_T^{miss} to establish the best limit on the inclusive cross section $\sigma(pp \to H^0 \to XX)$. As the signal in this case is suppressed by the requirement of high-P_T ISR jet, the limits are generally weak when compared to the RPV SUSY model and the 95% CL cross section limits are of the order of 1 pb or above under the assumption that the particle is stable. Extending this limit for finite lifetimes (the lifetime given in terms of $c\tau$), depending on the benchmark point, we found that our new results improve the published CMS limits for $c\tau$ above few metres in the best cases and for $c\tau$ above a kilometre in some worst case scenario, corresponding to lifetimes in the nanosecond to microsecond range. Furthermore, whilst the CMS displaced lepton/jet papers assume that the long-lived scalar particle X has specific decay modes, our analysis and the limit it gives are valid for any decay mode. This is an additional advantage of using the E_T^{miss} signatures to search for long-lived, neutral particles.

In the case of an RPV SUSY model, in which long-lived neutralinos are produced via squark decay, the 95% CL cross section limits obtained for stable particles, using the E_T^{miss} signal, are stronger than the corresponding limits obtained for the Higgs boson model, and can be as good as approximately 10 fb in case of a large mass splitting between the neutralino and squark. In this case the best limits generally come from ATLAS and CMS papers on multijet events in association with large E_T^{miss}. Also in this case, we then reinterpreted these results to produced upper limits for the inclusive cross section for $pp \to \tilde{Q}\tilde{Q} \to \tilde{\chi}^0\tilde{\chi}^0 +$ jets process as a function of the neutralino lifetime. Whilst we derived our limits assuming a specific RPV-SUSY model, as our limits do not depend on the decay channel of the neutralinos, these limits are valid for any SUSY model with the same production channel assuming negligible effect from heavy intermediate gluino exchange.

We summarise our results in two plots in the form of a m_{mediator} vs m_{LL} plane in figures 6 and 7. These plots are complemented with the respective tables 3 and 4 presented in the appendix. These tables containing limits for the grid in the m_{mediator} vs m_{LL} plane could be used for the interpretation of various new physics models obtaining the dependence on $c\tau$ by a similar procedure as described in section 2.4. Similar methods are planned to be used and the respective analysis are planned for LHC run II.

JHEP03(2016)018

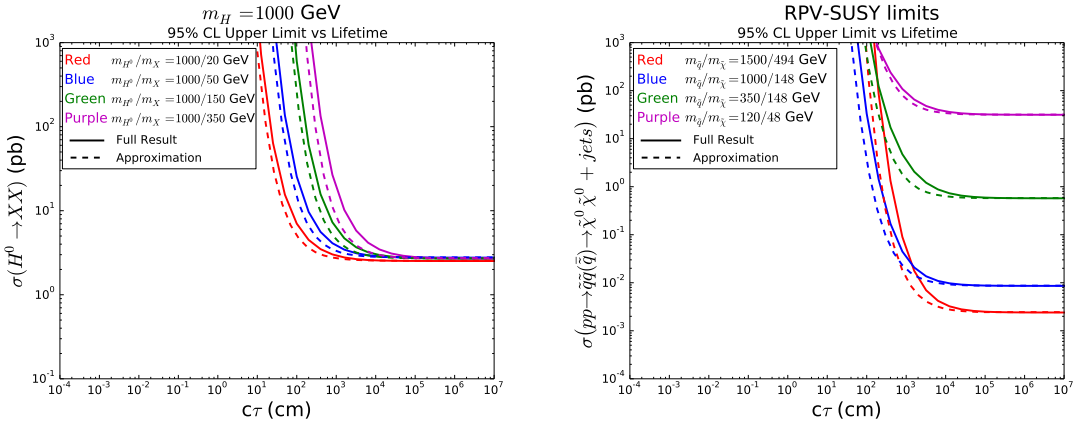

Figure 8. A comparison of limits derived using the exact method (solid) as described in the main text versus the approximation (dashed) described in appendix A.

Acknowledgments

AB, SM and MCT acknowledge partial support from the STFC grant number ST/L000296/1 and the NExT Institute. AB thanks the Royal Society Leverhulme Trust Senior Research Fellowship LT140094. MCT acknowledges support from an STFC STEP award. KN thanks SM for the hospitality and support he received at the U. of Southampton. He also acknowledges support from BMBF 00160287 *Comparing LHC Data with Beyond the Standard Model Physics*. AB and MCT also acknowledge partial funding by a Soton-FAPESP grant, and ICTP South American Institute for Fundamental Research (ICTP-SAIFR) in São Paulo support at the completion stage of the paper.

A Escape probability approximation

In section 2.4 we described a method to extrapolate $\sigma^{95\%}_{c\tau}$ from the cross section limit for stable particles, $\sigma^{95\%}_{\text{stable}}$, which is based on MC events only. There is however a simpler method to get the lifetime dependence, assuming that the LL particles are produced isotropically and their energies are not correlated. While these assumptions are not necessarily accurate, we found that this method leads to a 10-30% shift in the $c\tau$ variable in the $\sigma - c\tau$ exclusion plane as one can see from figure 8, where we present limits in this approximation and compare those with limits from figures 4–5 where we use the exact method described in section 2.4. This 10-30% shift in $c\tau$ leads to a very accurate (the same) limit for large $c\tau$ values. At the same time it leads to a potentially large (an order of magnitude) increase in the cross section limit for small values of $c\tau$ because of the exponential nature of the limit curves as one can see from figure 8.

Defining the distance that a LL particle travelled when it decays, $r = c\beta\gamma t$, and the mean decay distance, $D = c\beta\gamma\tau$, we have that the probability of decaying *beyond* a certain distance r is $\exp(-r/D)$. When we also take into account the $1/(4\pi r^2)$ drop due to increasing area, the probability of a particle crossing a small area S at a boundary at a

JHEP03(2016)018

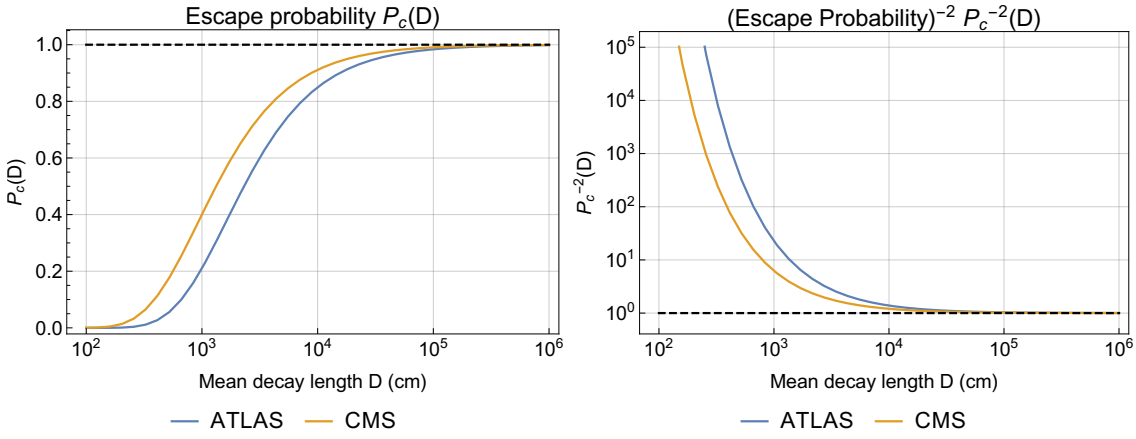

(a) (b)

Figure 9. Escape probability $P_{\rm c}(D = \beta\gamma c\tau)$ of long lived particles within a detector (left). On the right side, $P_{\rm c}^{-2}(D = \gamma c\tau)$ is shown.

distance r from the origin is

$$P(D) = \int_S f(r, D)\mathrm{d}S \tag{A.1}$$

with

$$f(r, D) = \frac{1}{4\pi r^2} \exp\left(\frac{-r}{D}\right). \tag{A.2}$$

In our case we wish to find the probability of a particle reaching beyond the boundary of a cylindrical detector, $P_{\rm c}(D)$. Splitting the cylinder into a barrel and endcaps, we have,

$$P_{\rm c}(D) = \int_{\rm barrel} f(r, D)\mathrm{d}S + \int_{\rm endcap} f(r, D)\mathrm{d}S \tag{A.3}$$

$$= 4\pi R \int_0^{L/2} f(\sqrt{z^2 + R^2}, D)\frac{R}{\sqrt{z^2 + R^2}}\mathrm{d}z \tag{A.4}$$

$$+ 4\pi \int_0^{R} f(\sqrt{(L/2)^2 + \rho^2}, D)\frac{L/2}{\sqrt{(L/2)^2 + \rho^2}}\rho\mathrm{d}\rho. \tag{A.5}$$

The function $P_{\rm c}(D)$ is universal and its numerical evaluation is shown in figure 9. To obtain a probability as a function of $c\tau$, we need to integrate over the relativistic factors $\beta\gamma = \sqrt{\gamma^2 - 1}$, or substituting $\gamma = E/m$, equivalently integrate over energy E. The integration has to be weighted with an energy distribution function, $g_m(E)$, which can be extracted from Monte Carlo simulation of events for each model and mass considered. The resulting function is $\bar{P}_{\rm c}(c\tau)$, which is also mass dependent because of the substitution $\gamma = E/m$.

$$\bar{P}_{\rm c}(c\tau) = \int \mathrm{d}E\, g_m(E)\, P_{\rm c}(D). \tag{A.6}$$

Since only the fraction of $\bar{P}_{\rm c}(c\tau)$ will contribute to the $E_T^{\rm miss}$ signature in case of unstable particles, we have the relation

$$\sigma_{c\tau}^{95\%} \times \bar{P}_{\rm c}(c\tau)^2 = \sigma_{\rm stable}^{95\%}, \tag{A.7}$$

JHEP03(2016)018

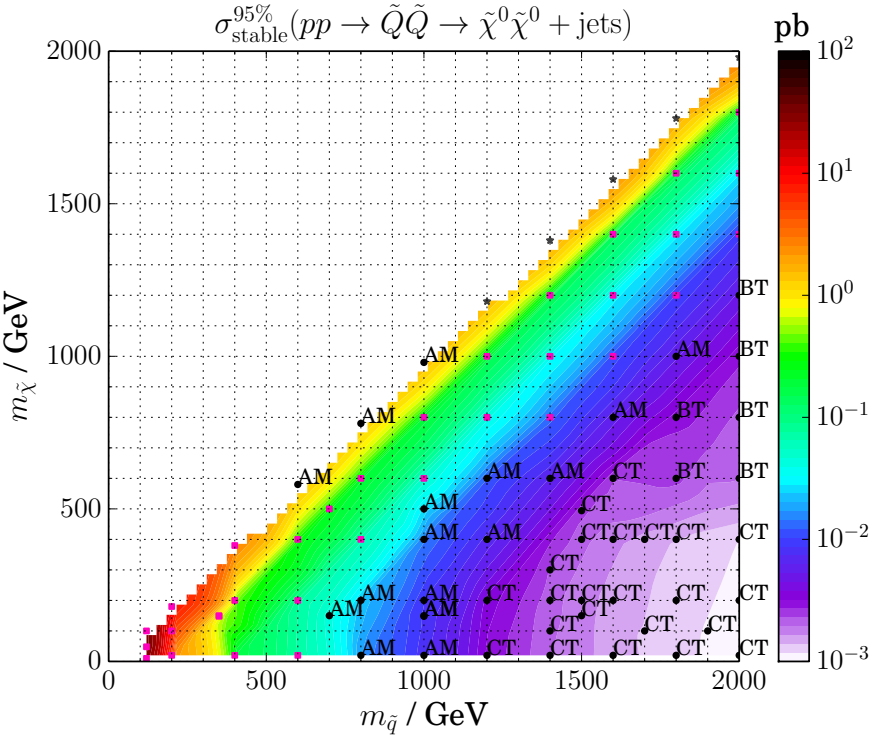

Figure 10. The figure shows the upper limit of the production cross section of $\tilde{\chi}^0\tilde{\chi}^0$+jets final states for the RPV-MSSM, similar to figure 7. The x-axis shows the mass of the $\tilde{q}$ squark and the y-axis shows the mass of the neutralino $\tilde{\chi}^0$. Black dots indicate sample points where the ATLAS multijet paper [29] performed best, grey stars indicate the ATLAS monojet paper [30], and pink squares indicate best performance with the CMS α_T paper [31]. Additionally, the analysis sets (signal regions) for the ATLAS multijet analyses are shown.

which can be rearranged into

$$\sigma^{95\%}_{c\tau} = \sigma^{95\%}_{\text{stable}} \times [\bar{P}_{\text{c}}(c\tau)]^{-2}. \tag{A.8}$$

This equation (A.8) provides the needed relation between $\sigma^{95\%}_{c\tau}$ and $\sigma^{95\%}_{\text{stable}}$.

B Tables

$m_{\tilde{q}}$ (GeV)	$m_{\tilde{\chi}}$ (GeV)	analysis	analysis set	$\sigma^{95\%}_{\text{stable}}$ (pb)
120	10	CMS α_T [31]	23j_0b_275	2.96e+01
120	48	CMS α_T [31]	4j_0b_325	3.35e+01
120	100	CMS α_T [31]	23j_0b_375	3.36e+01
200	20	CMS α_T [31]	23j_0b_275	2.46e+00
200	100	CMS α_T [31]	4j_0b_325	5.00e+00

JHEP03(2016)018

$m_{\tilde{q}}$ (GeV)	$m_{\tilde{\chi}}$ (GeV)	analysis	analysis set	$\sigma^{95\%}_{\text{stable}}$ (pb)
200	180	CMS α_T [31]	23j_0b_325	8.77e+00
350	148	CMS α_T [31]	23j_0b_325	5.73e-01
350	150	CMS α_T [31]	23j_0b_325	5.33e-01
400	20	CMS α_T [31]	23j_0b_375	1.71e-01
400	200	CMS α_T [31]	23j_0b_375	4.27e-01
400	380	CMS α_T [31]	23j_0b_375	2.68e+00
600	20	CMS α_T [31]	23j_0b_675	7.33e-02
600	200	CMS α_T [31]	23j_0b_475	7.74e-02
600	400	CMS α_T [31]	23j_0b_375	2.75e-01
600	580	ATLAS multijet [29]	AM	1.56e+00
700	150	ATLAS multijet [29]	AM	4.14e-02
700	500	CMS α_T [31]	23j_0b_375	2.43e-01
800	20	ATLAS multijet [29]	AM	1.62e-02
800	200	ATLAS multijet [29]	AM	2.24e-02
800	400	CMS α_T [31]	23j_0b_675	6.69e-02
800	600	CMS α_T [31]	23j_0b_375	2.15e-01
800	780	ATLAS multijet [29]	AM	1.39e+00
1000	20	ATLAS multijet [29]	AM	7.80e-03
1000	148	ATLAS multijet [29]	AM	8.56e-03
1000	150	ATLAS multijet [29]	AM	8.38e-03
1000	200	ATLAS multijet [29]	AM	8.68e-03
1000	400	ATLAS multijet [29]	AM	1.40e-02
1000	500	ATLAS multijet [29]	AM	2.54e-02
1000	600	CMS α_T [31]	23j_0b_675	4.80e-02
1000	800	CMS α_T [31]	23j_0b_375	1.87e-01
1000	980	ATLAS multijet [29]	AM	1.55e+00
1200	20	ATLAS multijet [29]	CT	3.05e-03
1200	200	ATLAS multijet [29]	CT	3.49e-03
1200	400	ATLAS multijet [29]	AM	6.89e-03
1200	600	ATLAS multijet [29]	AM	1.14e-02
1200	800	CMS α_T [31]	23j_0b_675	3.90e-02
1200	1000	CMS α_T [31]	23j_0b_375	1.60e-01
1200	1180	ATLAS monojet [30]	SR7	1.57e+00

JHEP03(2016)018

$m_{\tilde{q}}$ (GeV)	$m_{\tilde{\chi}}$ (GeV)	analysis	analysis set	$\sigma^{95\%}_{\text{stable}}$ (pb)
1400	20	ATLAS multijet [29]	CT	1.96e-03
1400	100	ATLAS multijet [29]	CT	2.02e-03
1400	200	ATLAS multijet [29]	CT	2.07e-03
1400	300	ATLAS multijet [29]	CT	2.25e-03
1400	600	ATLAS multijet [29]	AM	6.11e-03
1400	800	CMS α_T [31]	23j_0b_875	1.29e-02
1400	1000	CMS α_T [31]	23j_0b_675	3.44e-02
1400	1200	CMS α_T [31]	23j_0b_375	1.48e-01
1400	1380	ATLAS monojet [30]	SR8	1.94e+00
1500	150	ATLAS multijet [29]	CT	1.79e-03
1500	200	ATLAS multijet [29]	CT	1.76e-03
1500	400	ATLAS multijet [29]	CT	2.06e-03
1500	494	ATLAS multijet [29]	CT	2.40e-03
1600	20	ATLAS multijet [29]	CT	1.51e-03
1600	200	ATLAS multijet [29]	CT	1.53e-03
1600	400	ATLAS multijet [29]	CT	1.73e-03
1600	600	ATLAS multijet [29]	CT	2.31e-03
1600	800	ATLAS multijet [29]	AM	5.68e-03
1600	1000	CMS α_T [31]	23j_0b_875	1.11e-02
1600	1200	CMS α_T [31]	23j_0b_675	3.06e-02
1600	1400	CMS α_T [31]	23j_0b_375	1.38e-01
1600	1580	ATLAS monojet [30]	SR8	2.34e+00
1700	100	ATLAS multijet [29]	CT	1.35e-03
1700	400	ATLAS multijet [29]	CT	1.54e-03
1800	20	ATLAS multijet [29]	CT	1.23e-03
1800	200	ATLAS multijet [29]	CT	1.27e-03
1800	400	ATLAS multijet [29]	CT	1.38e-03
1800	600	ATLAS multijet [29]	BT	2.43e-03
1800	800	ATLAS multijet [29]	BT	2.97e-03
1800	1000	ATLAS multijet [29]	AM	5.39e-03
1800	1200	CMS α_T [31]	23j_0b_875	9.88e-03
1800	1400	CMS α_T [31]	23j_0b_675	2.84e-02
1800	1600	CMS α_T [31]	23j_0b_375	1.26e-01

JHEP03(2016)018

$m_{\tilde{q}}$ (GeV)	$m_{\tilde{\chi}}$ (GeV)	analysis	analysis set	$\sigma^{95\%}_{\text{stable}}$ (pb)
1800	1780	ATLAS monojet [30]	SR6	1.80e+00
1900	100	ATLAS multijet [29]	CT	1.17e-03
2000	20	ATLAS multijet [29]	CT	1.10e-03
2000	200	ATLAS multijet [29]	CT	1.13e-03
2000	400	ATLAS multijet [29]	CT	1.18e-03
2000	600	ATLAS multijet [29]	BT	1.99e-03
2000	800	ATLAS multijet [29]	BT	2.21e-03
2000	1000	ATLAS multijet [29]	BT	2.83e-03
2000	1200	ATLAS multijet [29]	BT	5.02e-03
2000	1400	CMS α_T [31]	23j_0b_875	9.19e-03
2000	1600	CMS α_T [31]	23j_0b_675	2.65e-02
2000	1800	CMS α_T [31]	23j_0b_375	1.21e-01
2000	1980	ATLAS monojet [30]	SR7	2.71e+00

Table 3. The complete grid scan result of the RPV-SUSY model.

m_H (GeV)	m_X (GeV)	analysis	analysis set	$\sigma^{95\%}_{\text{stable}}$ (pb)
100	10	ATLAS monojet [30]	SR4	5.77e+01
100	20	ATLAS monojet [30]	SR4	5.58e+01
100	50	ATLAS monojet [30]	SR4	5.38e+01
125	20	ATLAS monojet [30]	SR4	3.83e+01
125	50	ATLAS monojet [30]	SR4	3.99e+01
125	62	ATLAS monojet [30]	SR4	3.79e+01
200	10	ATLAS monojet [30]	SR4	1.67e+01
200	20	ATLAS monojet [30]	SR4	1.71e+01
200	50	ATLAS monojet [30]	SR4	1.75e+01
200	100	ATLAS monojet [30]	SR4	1.65e+01
400	10	ATLAS monojet [30]	SR6	3.26e+00
400	20	ATLAS monojet [30]	SR6	3.29e+00
400	50	ATLAS monojet [30]	SR6	3.17e+00
400	150	ATLAS monojet [30]	SR6	3.16e+00
400	200	ATLAS monojet [30]	SR6	3.12e+00
600	300	ATLAS monojet [30]	SR6	1.57e+00

JHEP03(2016)018

m_H (GeV)	m_X (GeV)	analysis	analysis set	$\sigma^{95\%}_{\text{stable}}$ (pb)
750	10	ATLAS monojet [30]	SR7	1.48e+00
750	20	ATLAS monojet [30]	SR7	1.61e+00
750	50	ATLAS monojet [30]	SR7	1.51e+00
750	150	ATLAS monojet [30]	SR7	1.48e+00
750	250	ATLAS monojet [30]	SR7	1.57e+00
750	300	ATLAS monojet [30]	SR7	1.49e+00
750	350	ATLAS monojet [30]	SR7	1.46e+00
750	375	ATLAS monojet [30]	SR7	1.46e+00
850	300	ATLAS monojet [30]	SR7	1.19e+00
850	400	ATLAS monojet [30]	SR7	1.22e+00
1000	10	ATLAS monojet [30]	SR7	9.31e-01
1000	20	ATLAS monojet [30]	SR7	9.39e-01
1000	50	ATLAS monojet [30]	SR7	9.55e-01
1000	150	ATLAS monojet [30]	SR7	9.41e-01
1000	250	ATLAS monojet [30]	SR7	9.64e-01
1000	350	ATLAS monojet [30]	SR7	9.67e-01
1000	500	ATLAS monojet [30]	SR7	9.69e-01
1200	150	ATLAS monojet [30]	SR8	8.00e-01
1200	250	ATLAS monojet [30]	SR8	8.32e-01
1200	300	ATLAS monojet [30]	SR8	8.11e-01
1200	350	ATLAS monojet [30]	SR8	7.85e-01
1200	400	ATLAS monojet [30]	SR8	8.30e-01
1200	450	ATLAS monojet [30]	SR8	7.93e-01
1200	600	ATLAS monojet [30]	SR8	8.11e-01
1500	10	ATLAS monojet [30]	SR8	6.17e-01
1500	20	ATLAS monojet [30]	SR8	6.33e-01
1500	50	ATLAS monojet [30]	SR8	6.10e-01
1500	150	ATLAS monojet [30]	SR8	6.27e-01
1500	250	ATLAS monojet [30]	SR8	6.32e-01
1500	350	ATLAS monojet [30]	SR8	6.41e-01
1500	500	ATLAS monojet [30]	SR8	6.32e-01
1500	750	ATLAS monojet [30]	SR8	6.47e-01
2000	10	ATLAS monojet [30]	SR8	4.90e-01

JHEP03(2016)018

m_H (GeV)	m_X (GeV)	analysis	analysis set	$\sigma^{95\%}_{\text{stable}}$ (pb)
2000	20	ATLAS monojet [30]	SR8	4.93e-01
2000	50	ATLAS monojet [30]	SR8	5.11e-01
2000	150	ATLAS monojet [30]	SR8	5.10e-01
2000	250	ATLAS monojet [30]	SR8	4.90e-01
2000	350	ATLAS monojet [30]	SR8	4.99e-01
2000	500	ATLAS monojet [30]	SR8	4.72e-01
2000	750	ATLAS monojet [30]	SR8	5.00e-01
2000	1000	ATLAS monojet [30]	SR8	5.06e-01

Table 4. The complete grid scan result of the HXX model.

References

[1] R. Barbier et al., *R-parity violating supersymmetry*, *Phys. Rept.* **420** (2005) 1 [hep-ph/0406039] [INSPIRE].

[2] J.L. Hewett, B. Lillie, M. Masip and T.G. Rizzo, *Signatures of long-lived gluinos in split supersymmetry*, *JHEP* **09** (2004) 070 [hep-ph/0408248] [INSPIRE].

[3] T. Han, Z. Si, K.M. Zurek and M.J. Strassler, *Phenomenology of hidden valleys at hadron colliders*, *JHEP* **07** (2008) 008 [arXiv:0712.2041] [INSPIRE].

[4] H.-C. Cheng and I. Low, *Little hierarchy, little Higgses and a little symmetry*, *JHEP* **08** (2004) 061 [hep-ph/0405243] [INSPIRE].

[5] H.-C. Cheng and I. Low, *TeV symmetry and the little hierarchy problem*, *JHEP* **09** (2003) 051 [hep-ph/0308199] [INSPIRE].

[6] C.T. Hill and R.J. Hill, *T^- parity violation by anomalies*, *Phys. Rev.* **D 76** (2007) 115014 [arXiv:0705.0697] [INSPIRE].

[7] L. Basso, A. Belyaev, S. Moretti and C.H. Shepherd-Themistocleous, *Phenomenology of the minimal B-L extension of the standard model: Z' and neutrinos*, *Phys. Rev.* **D 80** (2009) 055030 [arXiv:0812.4313] [INSPIRE].

[8] CMS collaboration, *Search for displaced supersymmetry in events with an electron and a muon with large impact parameters*, *Phys. Rev. Lett.* **114** (2015) 061801 [arXiv:1409.4789] [INSPIRE].

[9] CMS collaboration, *Search for long-lived particles that decay into final states containing two electrons or two muons in proton-proton collisions at $\sqrt{s} = 8$ TeV*, *Phys. Rev.* **D 91** (2015) 052012 [arXiv:1411.6977] [INSPIRE].

JHEP03(2016)018

[10] CMS collaboration, *Search for long-lived neutral particles decaying to quark-antiquark pairs in proton-proton collisions at* $\sqrt{s} = 8$ *TeV*, *Phys. Rev.* **D 91** (2015) 012007 [arXiv:1411.6530] [INSPIRE].

[11] ATLAS collaboration, *Search for massive, long-lived particles using multitrack displaced vertices or displaced lepton pairs in pp collisions at* $\sqrt{s} = 8$ *TeV with the ATLAS detector*, *Phys. Rev.* **D 92** (2015) 072004 [arXiv:1504.05162] [INSPIRE].

[12] ATLAS collaboration, *Search for pair-produced long-lived neutral particles decaying in the ATLAS hadronic calorimeter in pp collisions at* $\sqrt{s} = 8$ *TeV*, *Phys. Lett.* **B 743** (2015) 15 [arXiv:1501.04020] [INSPIRE].

[13] J. Alwall et al., *The automated computation of tree-level and next-to-leading order differential cross sections and their matching to parton shower simulations*, *JHEP* **07** (2014) 079 [arXiv:1405.0301] [INSPIRE].

[14] T. Sjöstrand, S. Mrenna and P.Z. Skands, *PYTHIA* 6.4 *physics and manual*, *JHEP* **05** (2006) 026 [hep-ph/0603175] [INSPIRE].

[15] P. Torrielli and S. Frixione, *Matching NLO QCD computations with PYTHIA using MC@NLO*, *JHEP* **04** (2010) 110 [arXiv:1002.4293] [INSPIRE].

[16] A.V. Semenov, *LanHEP: a package for automatic generation of Feynman rules in gauge models*, hep-ph/9608488 [INSPIRE].

[17] A.V. Semenov, *LanHEP: a package for automatic generation of Feynman rules in field theory. Version* 2.0, hep-ph/0208011 [INSPIRE].

[18] A. Semenov, *LanHEP — a package for automatic generation of Feynman rules from the Lagrangian. Updated version* 3.1, arXiv:1005.1909 [INSPIRE].

[19] M. Drees, H. Dreiner, D. Schmeier, J. Tattersall and J.S. Kim, *CheckMATE: confronting your favourite new physics model with LHC data*, *Comput. Phys. Commun.* **187** (2014) 227 [arXiv:1312.2591] [INSPIRE].

[20] DELPHES 3 collaboration, J. de Favereau et al., *DELPHES* 3*, a modular framework for fast simulation of a generic collider experiment*, *JHEP* **02** (2014) 057 [arXiv:1307.6346] [INSPIRE].

[21] M. Cacciari, G.P. Salam and G. Soyez, *FastJet user manual*, *Eur. Phys. J.* **C 72** (2012) 1896 [arXiv:1111.6097] [INSPIRE].

[22] M. Cacciari and G.P. Salam, *Dispelling the* N^3 *myth for the* k_t *jet-finder*, *Phys. Lett.* **B 641** (2006) 57 [hep-ph/0512210] [INSPIRE].

[23] M. Cacciari, G.P. Salam and G. Soyez, *The anti-*k_t *jet clustering algorithm*, *JHEP* **04** (2008) 063 [arXiv:0802.1189] [INSPIRE].

[24] A.L. Read, *Presentation of search results: the* CL_s *technique*, *J. Phys.* **G 28** (2002) 2693 [INSPIRE].

[25] C.G. Lester and D.J. Summers, *Measuring masses of semiinvisibly decaying particles pair produced at hadron colliders*, *Phys. Lett.* **B 463** (1999) 99 [hep-ph/9906349] [INSPIRE].

[26] A. Barr, C. Lester and P. Stephens, m_{T2}*: the truth behind the glamour*, *J. Phys.* **G 29** (2003) 2343 [hep-ph/0304226] [INSPIRE].

[27] H.-C. Cheng and Z. Han, *Minimal kinematic constraints and* m_{T2}, *JHEP* **12** (2008) 063 [arXiv:0810.5178] [INSPIRE].

JHEP03(2016)018

[28] CMS collaboration, *Search for dark matter, extra dimensions and unparticles in monojet events in proton-proton collisions at* $\sqrt{s} = 8$ *TeV*, *Eur. Phys. J.* **C 75** (2015) 235 [arXiv:1408.3583] [INSPIRE].

[29] ATLAS collaboration, *Search for squarks and gluinos with the ATLAS detector in final states with jets and missing transverse momentum and* $20.3\,\text{fb}^{-1}$ *of* $\sqrt{s} = 8$ *TeV proton-proton collision data*, ATLAS-CONF-2013-047, CERN, Geneva Switzerland (2013).

[30] ATLAS collaboration, *Search for new phenomena in final states with an energetic jet and large missing transverse momentum in pp collisions at* $\sqrt{s} = 8$ *TeV with the ATLAS detector*, *Eur. Phys. J.* **C 75** (2015) 299 [*Erratum ibid.* **C 75** (2015) 408] [arXiv:1502.01518] [INSPIRE].

[31] CMS collaboration, *Search for supersymmetry in hadronic final states with missing transverse energy using the variables* α_T *and b-quark multiplicity in pp collisions at* $\sqrt{s} = 8$ *TeV*, *Eur. Phys. J.* **C 73** (2013) 2568 [arXiv:1303.2985] [INSPIRE].

[32] L. Randall and D. Tucker-Smith, *Dijet searches for supersymmetry at the LHC*, *Phys. Rev. Lett.* **101** (2008) 221803 [arXiv:0806.1049] [INSPIRE].

[33] CMS collaboration, *Search for supersymmetry in pp collisions at 7 TeV in events with jets and missing transverse energy*, *Phys. Lett.* **B 698** (2011) 196 [arXiv:1101.1628] [INSPIRE].

JHEP03(2016)018